Lettau, H. H., "A re-examination of the 'Leipzig wind profile'," *Tellus* **2,** 125–129 (1950).
Lettau, H. H., "Wind profile, surface stress, and geostrophic drag coefficients in the atmospheric surface layer," *Adv. Geophys.* **6,** 241–257 (1959).
Lumley, J. L. and Panofsky, H. A., "The structure of atmospheric turbulence," *Monographs and texts in physics and astronomy*, Vol. XII Interscience (1964).
Mellor, G. L., Chapple, P. J. and Stokes, V. K., "On the flow between a rotating and a stationary disk," *J. Fluid Mech.* **31,** 95–112 (1968).
Munn, R. E., "Descriptive micrometeorology," supplement to *Advances in Geophysics*, Academic Press (1966).
Rossby, C. G. and Montgomery, R. B., "The layer of frictional influence in wind and ocean currents," *Papers Phys. Oceanogr. Meteor.*, M.I.T. and Woods Hole Oceanogr. Inst. **3,** 101–108 (1935).
Spence, D. A. and Brown, G. L., "Heat transfer to a quadratic shear profile," *J. Fluid Mech.* **33,** 753–773 (1968).
Swinbank, W. C., "Structure of wind and the shearing stress in the planetary boundary layer," *Arch, Met. Geoph. Biokl. Ser. A*, **19,** 1–12 (1970).
Taylor, G. I., "Eddy motion in the atmosphere," *Phil. Trans. Roy. Soc.* London A215, 1–26 (1915).
Taylor, P. A., "On planetary boundary layer flow under conditions of neutral thermal stability," *J. Atmos. Sci.* **26,** 427–431 (1969).
Van Atta, C. W. and Chen, W. Y., "Measurements of spectral energy transfer in grid turbulence," *J. Fluid Mech.* **34,** 497–513 (1968).
Wyngaard, J. C., "Measurement of small-scale turbulence structure with hot wires," *J. Sci. Inst., Series* 2 **1,** 1105–1108 (1968).
Yajnik, K. S., "Asymptotic theory of turbulent shear flows," *J. Fluid Mech.* **42,** 411–427 (1970).
Yamamoto, G., Yasuda, N. and Shimanuki, A., "Effect of thermal stratification on the Ekman layer," *J. Meteor. Soc. Japan* **46,** 442–454 (1968).

Geophysical Fluid Dynamics, 1972, Vol. 3, pp. 161–180
© 1972 Gordon and Breach Science Publishers Ltd.
Printed in Great Britain

Observations of Rapid Mean Flow Produced In Mercury By a Moving Heater†

J. A. WHITEHEAD

Institute of Geophysics and Planetary Physics
University of California, Los Angeles‡

(*Received June 30, 1971*)

Experimental and theoretical results are described for the moving flame experiment, where a heat source moves under a horizontal, annular channel filled with liquid mercury. The physical range under discussion consists of the creep flow limit, in which inertial forces are less than viscous forces. A mean surface flow was observed on the mercury. This flow was up to four times greater than the heater speed, and in an opposite direction. The ratio of mean flow to heater speed was theoretically and experimentally found to be proportional to the square of the thermal amplitude, in agreement with a special limit of Davey's earlier results. The basic flow here, as contrasted to those flows analyzed by earlier theories, appears to be generated by surface tension. However, the Reynolds stress mechanism which generates the mean flow is the same. Some experimental flows were so rapid that the range of validity of the present, as well as some earlier theories, was exceeded. The present theory suggests that the higher order nonlinearities may have cancellative effects, which implies that the present and some earlier theories are valid beyond their normal range of validity.

1. Introduction

This paper concerns itself with the moving flame experiment, in which a horizontal annular channel of fluid is subjected to a heat source moving at a constant speed under the channel. The resulting circulation of the fluid generates a net Reynolds stress which produces a mean flow. It is therefore a cousin to many atmospheric processes which generate a mean stress (see V. P. Starr "Negative Viscosity" (1968)), and also a cousin to acoustic streaming. Its utility, outside of the many obvious applications in geophysics,

† Contribution No. 850, Institute of Geophysics and Planetary Physics, University of California, Los Angeles.

‡ Present address: Woods Hole Oceanographic Institution, Woods Hole, Massachusetts.

biology, and engineering, arises because momentum convection can be systematically observed, measured, and compared with analytic predictive schemes in hopes of generating new understanding of more complicated flow processes.

The emphasis here will be upon comparing experimental results with theoretical predictions for low Prandtl number fluid. As the "creep flow" limit is exceeded, so that inertia becomes as large as viscous momentum transport, the experiments generate flows which are not only many times greater than any previous experimental studies, but are also many times greater than those predicted from existing theories. In addition, some data exceed the limits of validity of any theoretical predictions presently in the literature, in virtue of the fact that the flow can be more rapid than the flame speed itself. Therefore, the experimental data is accompanied by a theoretical analysis for both buoyancy and surface tension driven flows, in the course of which it appears that the experimentally driven flows reported here, as well as those reported by some others, are generated by surface tension circulations. Happily, the mechanism for generating the mean flows appears to be identical to that of the buoyancy driven circulations, so that analogies can clearly be drawn. Finally, the equations are pursued to higher orders to assess the next order mean flow.

Experimental studies by Fultz (1956) first isolated the moving flame effect in a pan of water heated below by a rotating flame. Stern (1959) carried out a similar series of experiments in an annulus and observed flows with velocities up to 1 % the speed of the flame, and in an opposite direction. The theoretical study by Davey (1967) used a weak nonlinear approximation to the Navier–Stokes equation to study buoyancy driven circulation. He, like Stern, pointed out the role played by the finite time it takes vorticity and temperature to diffuse through the fluid. He expressed the opinion that the most significant effect comes from slow thermal diffusion. Our results seem to contradict this in that low Prandtl number mercury diffuses heat approximately forty times as effectively as it diffuses vorticity, and yet leads to flows 400 times greater than those previously observed.

The need for more analysis of the moving flame problem has been stimulated by Schubert (1969), who noted that in the limit of small Prandtl number and for sufficient heating, the calculations of Davey predicted flow which was more rapid than the flame speed, and which was in an opposite direction. Unfortunately, Davey's analysis was not strictly valid for rapid flows, nor had Fultz and Stern reported such rapid flows in water. Being motivated to determine whether this phenomenon could possibly create a circulation in the upper atmosphere of Venus, Schubert used a numerical technique to find the flow behavior. The computations predicted that the flows could go at roughly the flame speed before some apparently difficult calculational

problems occurred. Experiments with liquid mercury by Schubert and Whitehead (1969) confirmed that rapid flows existed by generating surface flows in the mercury going up to four times faster than the flame and in the opposite direction. Since that time, theories have predicted rapid mean flows (Hinch and Schubert (1970)), and even predictions of mean flows from a stationary flame have been made (Malkus (1970), Thompson (1970)). This paper continues the study of such rapid flows in mercury. The experimental observations will be discussed in the next section with the theoretical analysis following that.

2. Experiments with liquid mercury

The experiments to be reported here have been conducted using an annular channel containing liquid mercury, as shown from above in figure 1. A heat

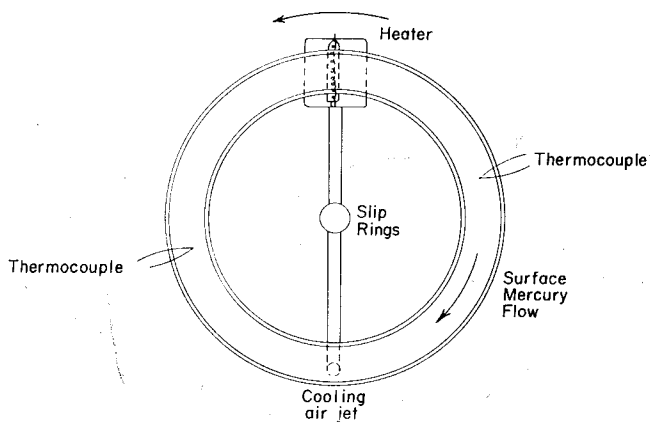

FIGURE 1 Schematic view of the apparatus from above.

source travelled under the channel. In early experiments this was a bunsen flame, although it was soon replaced by a 500-watt lamp. The top of the mercury was exposed, permitting measurements to be taken of its temperature and velocity.

Various physical considerations determined the design of the channel. In order to eliminate spurious flows, the bottom of the channel was made flat to within 0.02 mm, and the annulus leveled to within 0.01 mm. The channel itself had a rectangular cross section and was made of anodized aluminum. The dimensions were a compromise between the limited amount of mercury available (about one-half liter) and the following physical constraints: A small rotational force in the fluid, which would ideally require a

large radius; two-dimensional flow, which would ideally require a wide channel; and flexibility in the vertical depth of the mercury, which would ideally require a deep channel. The final dimensions selected were 2.5 cm deep × 2.5 cm wide × 10 cm radius, machined to ±0.002 cm. The effect of rotation of the mercury for some of the deeper experiments was important, as will be discussed later.

The channel was heated by a 500-watt, quartz–iodine light bulb which rotated below the channel. Its power was controlled by a variable voltage source. Halfway around the channel a jet of air was directed upward to serve as a heat sink and cool the channel. Both the heat source and sink were connected to a gear box and a synchronous motor which propelled the source and sink at a constant speed under the annulus. The thickness of the bottom of the aluminum channel was 0.2 cm, which assured good heat transfer to the fluid above. Mercury was poured into the channel, and was then covered with a thin layer of distilled water to retard oxidation. It was found that a layer of relatively rigid oxide accompanied the mercury. Therefore, the surface of the mercury had to be vacuumed before the experiment began. Depth of the mercury was determined by using a micrometer depth gauge with a pointed tip. It was found that the surface of the mercury was abruptly deformed as the tip, being fed down, made contact. One could easily measure the position of the top surface of the mercury to within ±0.001 cm by viewing the sudden distortion of a reflected straight line. A transparent cover of plexiglass was placed over the channel to eliminate unwanted air currents from the room. It was wound with electrical heating wires which inhibited the condensation of water vapor. The apparatus was placed in a fume hood to prevent any accidental inhalation of mercury vapors.

Flow on top of the mercury was visualized by observing the movement of small air bubbles which condensed on the water–mercury interface. This was the most convenient method of measuring velocity that was found, so a number of experiments were performed to determine whether these surface bubbles moved as a result of motions in the mercury, or whether they moved as a result of motions of the water. In the first set, dyes were injected into the water above the mercury, and the depth of the water was systematically varied to see if the water contributed any shear forces downward into the mercury. It was found that the water transmitted negligible shear. In addition, varying the water depth did not measurably change the bubble velocities, and the vertical and horizontal rates of shear in the water were less than 5% of the shear in the mercury. Essentially, the water layer followed the top surface of the mercury.

A second experiment was run to infer flows within the mercury. A carefully balanced vertical metal rod was made with a low-friction pivot slightly above its center of gravity. The tip of this rod, when placed in a moving fluid, was swept slightly downstream in proportion to the arithmetic mean of the flow. This tilted the rod. The device was calibrated, and measurements of the mean flow were recorded. Surface velocities of the bubbles agreed well with the mean flow of the interior of the mercury. Therefore, the principal measurements discussed subsequently are the times of surface bubbles to go 1 cm. Additional measurements were obtained by using lacquer-covered, 30-gauge (0.025 cm), copper–constantin thermocouples.

The apparatus permitted one to have quantitative control over all the important variables. This is in contrast to the early exploratory studies of Schubert and Whitehead (1969) in which the variables were only roughly known. The temperature, although not a pure sine curve, could be reconciled with the analytical predictions to be discussed in Part 3 by a Fourier analysis of the thermal field.

Data for the various experimental runs are listed in table I. Velocity was recorded five minutes after the heater was turned on. The velocity of the upper surface of the fluid was determined by timing the passage of surface bubbles for a one-centimeter traverse. Twelve or more such readings were taken at equally spaced intervals during at least two consecutive rotations of the heat source. The datum points were then graphically plotted, and if the data from the two cycles showed qualitative agreement, an average was taken of their value, which is recorded in column 7. A typical velocity vs. time plot is shown in figure 2. In the upper curve the mean surface velocity was of the order of the fluctuating surface velocity, so that bubble flows were almost always in one direction (except for a small region behind the heater). Such experiments gave the clearest results. However, the experiments with the slowest mean flows invariably had large fluctuating flows, as shown in the lower curve which made measurements of the mean motion much less accurate. In the case of the slowest flows, when heater speed was 0.8 cm/second, it was necessary to adopt a different measurement procedure and record the amount of advance of a single bubble during one heater rotation. In that particular case the bubble would only advance a few millimeters for each traverse, and so errors on the order of 50% can be expected in that particular data. Although this technique measured the Lagrangian mean flow rather than the Eulerian mean flow, it was observed that all flows in these cases were less than the flame speed, so that laterial bubble displacements were small, and the two measurements were approximately equivalent.

The temperatures reported were the peak-to-peak values as recorded by a thermocouple at the bottom of the mercury channel. Since the heaters were located below the channel, these values of temperature were found to be greater than the mean values in the interior of the mercury due to the finite conductivity of the mercury. To assess the influence of this conduction, use was made of the equation $U(\partial T/\partial x) = \kappa(\partial^2 T/\partial z^2)$, where T is temperature,

U is velocity of the moving heater, κ is thermal diffusivity of the mercury, x is direction of heater movement, and z is the direction of gravity. Assuming there is a temperature boundary condition specified at $z = 0$ of the form

TABLE I

Run Number	Ucm/sec	T_{max}-T_{min}	C_1	T°C	Lcm	$\bar{u}/U$
1	0.8	8.5	0.85	3.61	0.35	0.010
2	0.8	8.5	0.85	3.61	0.35	0.015
3	0.8	9.0	0.85	3.82	0.35	0.015
4	0.8	13.0	0.85	5.53	0.35	0.020
5	0.8	13.0	0.85	5.53	0.35	0.027
6	0.8	13.0	0.85	5.53	0.35	0.034
7	0.8	17.0	0.85*	7.23	0.35	0.087
8	0.45	27.0	0.89	11.56	0.35	0.27
9	0.3	31.0	0.91	13.81	0.35	0.22
10	0.15	23.0	0.93	10.71	0.35	0.21
11	0.15	29.0	0.93	13.51	0.35	0.25
12	0.15	35.0	0.93	16.31	0.35	0.40
13	0.15	39.0	0.93	18.17	0.35	0.57
14	0.15	44.0	0.93	20.52	0.35	0.57
15	0.15	43.0	0.93	18.00	0.35	0.60
16	0.15	53.0	0.93	22.47	0.35	0.67
17	0.15	60.0	0.93	25.44	0.35	0.70
18	0.15	57.0	0.93	24.16	0.35	0.74
19	0.10	31.0	0.95	14.74	0.35	0.26
20	0.10	40.0	0.95	19.02	0.35	0.4
21	0.10	62.0	0.95	29.49	0.35	0.7
22	0.05	38.0	0.97	18.46	0.35	0.37
23	0.15	45.0	0.95	21.40	0.50	0.87
24	0.15	21.0	0.87	8.94	0.70	0.54
25	0.15	25.0	0.87	12.43	0.70	0.86
26	0.15	39.0	0.87	16.60	0.70	1.2
27	0.15	24.0	0.75*	9.00	1.5	2.7
28	0.15	31.0	0.75*	11.63	1.5	4.0
29	0.15	39.0	0.75*	14.64	1.5	4.5

$T = \sin kx$, and all solutions decay as $z \to \infty$, the solution is of the form $\sin(kx+pz)e^{-pz}$, where p is proportional to $\sqrt{(Uk/\kappa)}$. If $\sqrt{(\kappa/Uk)} > L$, the depth of the fluid, the approximate average temperature of the fluid is

$$\left(1-\frac{L}{2}\sqrt{\frac{Uk}{\kappa}}\right)T(0).$$

The estimated correction due to thermal conductivity in the experiment is labeled "C_1" in table I and was found from the extreme values, labeled with a star, which were directly measured by placing a number of thermocouples at various depths in the mercury and determining its average temperature.

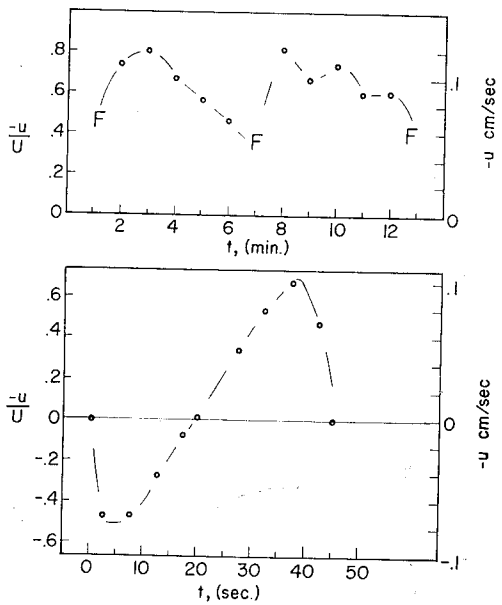

FIGURE 2 Surface velocity of mercury as a function of time. The upper data is run number 15 on Table 1 with $\bar{u}/U = 0.6$. Note that the mean flow is somewhat greater than the fluctuating flow. The lower data is run number 3 on Table 1 with $\bar{u}/U = 0.015$. Measurements for those low values of $\bar{u}/U$ are subject to large experimental errors because the fluctuating flows are much larger than the mean flow.

The intermediate values of C_1 were taken from the formula $C_1 = 1 - L\sqrt{(U)}(1-C_1^*)/L^*\sqrt{(U^*)}$, which was motivated by the solution to the one-dimensional, time-dependent, heat conduction equation which was discussed above. Values ranged from 0.75 to almost 1.00.

Detailed comparison of experiment and theory will be done after the theoretical section. We note here only that mean surface flows up to four times the speed of the flames were observed. One last measurement was useful in formulating the problem. It was suggested by Davey that these mean flows arose because of a thermal tail in the temperature field. At the speeds of this experiment two temperature traces are shown in figure 3, one taken near the top of 1.5 cm deep mercury, and the other taken near the bottom. These traces show various things. First, the shape of the thermal field is quite similar at

various depths of the mercury. Second, the amplitude of the thermal signal is less near the top of the mercury, which verifies the discussion in the previous paragraph. Third, the phase lag of the thermal field from the top to the bottom is only about 4 or 5%.

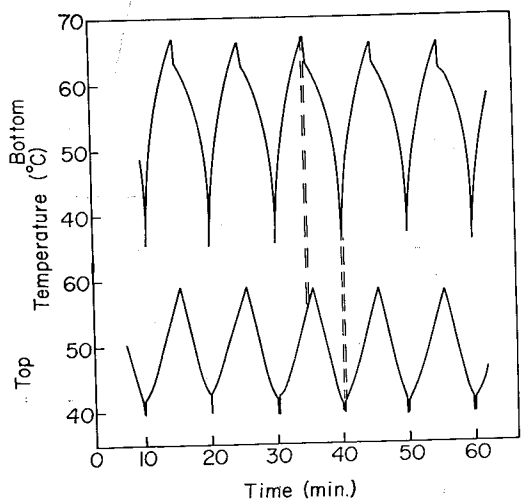

FIGURE 3 Temperature of the mercury as the heater passes. Note the very minor difference in the temperatures at the top of the mercury and at the bottom due to the relatively good thermal conductivity of mercury. The mean flow at the top of the mercury compared to the heater speed was approximately one.

Estimates of the Reynolds stress from such a lag indicated it was far too small to produce flows of the observed magnitude. In fact, measurements indicated that there was a much greater velocity (or vorticity) phase lag due to the fact that vorticity diffuses more slowly than temperature. This will be used in the low Prandtl number analysis to be developed next.

3. Linearized theory

3.1. Formulation

The Boussinesq approximations to the conservation of mass, momentum, and energy are

$$\nabla\cdot\mathbf{u} = 0, \tag{3.1.1}$$

$$(\partial\mathbf{u}/\partial t)+\mathbf{u}\cdot\nabla\mathbf{u} = -(1/\rho)\nabla p+\nu\nabla^2\mathbf{u}+g\alpha T\hat{k}, \tag{3.1.2}$$

$$(\partial T/\partial t)+\mathbf{u}\cdot\nabla T = \kappa\nabla^2 T, \tag{3.1.3}$$

Where $\mathbf{u}$, p and T are velocity, the deviation from hydrostatic pressure, and temperature; and ν, κ, g, α are kinematic viscosity, thermal diffusivity, force of gravity, and the volumetric coefficient of expansion, respectively. $\hat{k}$ is a unit vector in the plus z (upward) direction. Boundary conditions on temperature are

$$T = \Delta T \sin (1/R)(x+vt) \text{ at } z = \pm L/2 \tag{3.1.4}$$

where v is velocity of the heater while L and R are vertical depth and radius of the annulus, respectively. The effects of buoyancy and surface tension driven flows will be investigated in the limit of long wavelength and low Prandtl number fluid using the transforms:

$$u_d = \frac{\nu}{R}\frac{\partial\psi_n}{\partial z_n} \qquad w_d = -\frac{\nu L}{R^2}\frac{\partial\psi_n}{\partial x_n}$$

$$t_d = \frac{R^2}{\nu}t_n \qquad T_d = \Delta T\, T_n$$

$$x_d = Rx_n \qquad z_d = Lz_n,$$

where subscripts d and n stand for dimensional and non-dimensional values. Equations 3.1.1–4 reduce to the following dimensionless forms, where the subscripts n will henceforth be deleted:

$$\left[a^2\frac{\partial}{\partial t}-\nabla_1^2\right]\nabla_1^2\psi+G\frac{\partial T}{\partial x} = a^2 J(\psi, \nabla_1^2\psi), \tag{3.1.5}$$

$$a^2 P_r\left[\frac{\partial T}{\partial t}-J(\psi, T)\right] = \nabla_1^2 T, \tag{3.1.6}$$

$$T = \sin (x+Ut), \tag{3.1.7}$$

where

$$\nabla_1^2 \equiv \left(a^2\frac{\partial^2}{\partial x^2}+\frac{\partial^2}{\partial z_1^2}\right), \quad a \equiv L/R, \quad G \equiv \frac{g\alpha L^3\Delta T}{\nu^2}, \quad P_r \equiv \nu/\kappa,$$

$$U \equiv vR/\nu, \quad J(A, B) \equiv \frac{\partial A}{\partial x}\frac{\partial B}{\partial z}-\frac{\partial A}{\partial z}\frac{\partial B}{\partial x}.$$

The formal procedure to obtain solutions to these nonlinear equations will be to assume "a" small and expand velocity and temperature in asymptotic series of a^2, i.e. set $\psi = \psi_0+a^2\psi_1+a^4\psi_2+\ldots$, $T = T_0+a^2T_1+\ldots$. The

appropriateness of this expansion for the examples which are to be compared with experiment will be justified *a posteriori*, as integration of successive solutions will generate small coefficients. By varying boundary conditions, a variety of different circumstances are generated.

3.2. Buoyancy Generated Flows

In order to demonstrate the method of solution and to seek the influence of higher orders, we will first seek solutions for the vertically symmetric, rigid-surface boundary conditions $\partial\psi/\partial x = \partial\psi/\partial z = 0$ at $z = \pm\frac{1}{2}$. Lowest order in equations 3.1.6 and 3.1.5 are

$$\partial^2 T_0/\partial z^2 = 0 \tag{3.2.1}$$

and

$$-\frac{\partial^4\psi_0}{\partial z^4} + G\frac{\partial T_0}{\partial x} = 0. \tag{3.2.2}$$

Using the temperature boundary condition equation (3.1.7), the above equations yield the solutions

$$T_0 = \sin(x+Ut), \tag{3.2.3}$$

and

$$\psi_0 = (Gg_4/4!)\cos(x+Ut). \tag{3.2.4}$$

where

$$g_n \equiv z^n - \frac{nz^2}{2^{n-1}} + \frac{n-2}{2^{n+1}} \quad \text{for } n \text{ even},$$

$$g_n \equiv z^n - \frac{(n-1)z^3}{2^{n-2}} + \frac{(n-3)z}{2^n} \quad \text{for } n \text{ odd}.$$

These are polynomials which fit zero velocity boundary conditions.

To order a^2 there will be no mean flow generated. To order a^4 a mean flow will be generated by ψ_0 interacting in the Jacobian with that portion of ψ_1 which has a $\sin(x+Ut)$ dependence. Those portions of equations 3.1.6 and 3.1.5 which generate such terms to order a^2 are

$$\frac{\partial^2 T_1}{\partial z^2} = \mathrm{Pr}\frac{\partial T_0}{\partial t} \tag{3.2.5}$$

and

$$\frac{\partial^4\psi_1}{\partial z^4} = \frac{\partial}{\partial t}\frac{\partial^2\psi_1}{\partial z^2} + G\frac{\partial T_1}{\partial x}. \tag{3.2.6}$$

Boundary conditions are that temperature and velocity are zero to order a^2, and so solutions are,

$$T_1 = \tfrac{1}{2}PrU(z^2 - 1/4)\cos(x+Ut) \tag{3.2.7}$$

and

$$\psi_1 = -GU\left[\frac{Pr+1}{6!}g_6 - \frac{3Pr+1}{(4!)^2}g_4\right]\sin(x+Ut). \tag{3.2.8}$$

Assuming steady flow to order a^4, a zeroth harmonic is generated from the formula

$$\frac{\partial^4\psi_2}{\partial z^4} = -J\left(\psi_0, \frac{\partial^2\psi_1}{\partial z^2}\right) - J\left(\psi_1, \frac{\partial^2\psi_0}{\partial z^2}\right). \tag{3.2.9}$$

The Jacobian operators express the convection of momentum, and produce a second harmonic $\cos 2(x+Ut)$, which is a rudimentary boundary layer, and a zeroth harmonic $\cos 0(x+Ut)$, which is a preferential accumulation of momentum in the interior of the fluid. The stress budget is illustrated in figure 4. The 0(1) velocity (solid arrows) feeds momentum from the $0(a^2)$ velocity (dotted arrows) into the interior. This momentum is in an anti-flame direction. Conversely, a quarter wavelength down the tank the $0(a^2)$ velocity feeds a smaller momentum from the 0(1) velocity into the interior. This momentum is in a flame direction. Stress generating the mean flow is the sum of these accumulations, while stress generating the second harmonic is the difference. F. Busse has pointed out, in conversation, that there is an exact solution to a different set of boundary conditions where the nonlinear interactions are exactly zero, and so figure 4 does not hold in general for all circulating fluids. Instead, it is a consequence of the fact that the polynomials in the z direction contain more than one Fourier component.

Denoting by an overbar the mean flow potential (which is the zeroth harmonic) we find

$$\bar{\psi}_2 = -\frac{G^2U(1+Pr)}{6!4!}\left[\frac{z^{11}}{11\cdot 10} - \frac{z^9}{18\cdot 2^2} + \frac{1}{7\cdot 2^4}z^7 - \frac{1}{5\cdot 2^6}z^5 + \frac{1}{6\cdot 2^8}z^3 - \frac{1}{10\cdot 2^{10}}z\right] \tag{3.2.10}$$

The second order boundary conditions for this are $\psi_z = \psi_{zz} = 0$ at $z = \pm\frac{1}{2}$, the latter found by noting that for steady flow the average tangential stress at the boundary must be zero, as that is the only external force in the

x-direction which acts on the fluid. Denoting the average over x and z by brackets, the mean flow is found to be

$$\frac{\langle u\rangle}{U} = \frac{(Pr+1)}{12!}\, G^2 a^4 \tag{3.2.11}$$

a result identical to that obtained by Davey in the limit Ua^2 small.

In the transient state the fluid acquires its net momentum in the x-direction through friction. This can easily be seen by investigating the

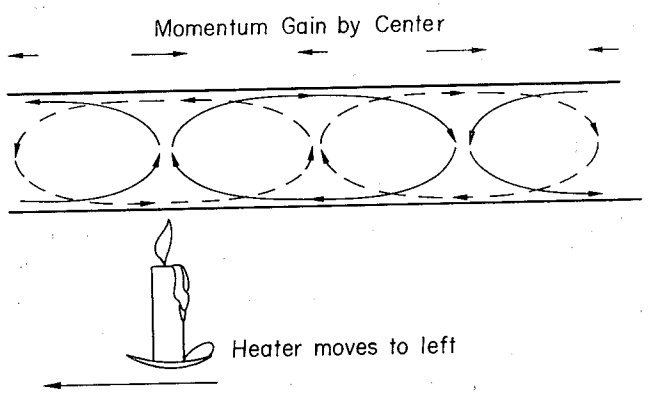

FIGURE 4 Lowest order net momentum transfer. The $0(a^2)$ circulation (dotted arrows) feeds momentum from the 0(1) circulation into the interior. The second harmonic is generated because the 0(1) velocity feeds an opposed, but smaller, momentum from the $0(a^2)$ term into the interior.

generation of mean flow from rest by assuming that the zeroth and first order flows are fully developed, as given in equations (3.2.4) and (3.2.8). We wish to rescale time so that the time derivative is of order one, so we define $t = a^2 t'$. The equation for generating a mean flow is

$$\frac{\partial}{\partial t'}\frac{\partial^2 \psi_2}{\partial z^2} = J\left(\psi_0, \frac{\partial^2 \psi_1}{\partial z^2}\right) + J\left(\psi_1, \frac{\partial^2 \psi_0}{\partial z^2}\right).$$

Using the boundary condition $\partial \bar{\psi}_2/\partial z = 0$ at $z = \pm \frac{1}{2}$, one gets

$$\frac{\partial \bar{\psi}_2}{\partial t'} = \frac{G^2 U(1+Pr)}{6!4!}\left[z^9 - z^7 + \frac{3}{8}z^5 - \frac{1}{8}z^3 + \frac{13}{2^8}z\right] \tag{3.2.12}$$

Acceleration is

$$\frac{\partial}{\partial t'}\frac{\bar{u}}{U} = \frac{G^2(1+Pr)}{6!4!}\left[9z^8 - \frac{28}{2^2}z^6 + \frac{30}{2^4}z^4 - \frac{24}{2^6}z^2 + \frac{13}{2^8}\right]a^4, \tag{3.2.13}$$

and is sketched as a function of z in figure 5.

Average mean flow increase is

$$\frac{1}{U}\frac{\partial \langle u\rangle}{\partial t} = \frac{G^2(1+Pr)}{6!4!2^5}\, a^4. \tag{3.2.14}$$

One finds no new contribution to the mean flow equation to order a^6. For zero Prandtl number the order a^8 mean flow is found to be

$$\langle u\rangle/U = 1/12!\,[G^2a^4 - 0.0024\, G^2U^2a^8 + 0(10^{-8})G^4a^8]. \tag{3.2.15}$$

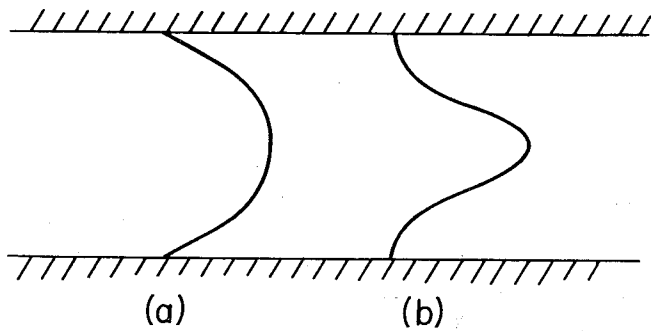

FIGURE 5 Sketch of (a) acceleration (eq. 3.2.8) from rest with rigid boundary conditions and (b) final velocity (eq. 3.2.5). Acceleration magnitude is approximately 100 times greater than the final velocity magnitude.

The $G^2U^2a^8$ correction arises from additional temporal lags which would not arise if the slow heater speed assumption had not been made. The corrections tend to decrease the mean flow. The G^4a^8 corrections were found by a computer to be 1.1×10^{-8}, with a possible error of almost the same size, so the correction in equation (3.2.15) is only shown to be of order 10^{-8}. Various mechanisms generated these corrections, the two principal ones being additional vorticity phase lag generated by the mean flow, and more efficient momentum transport to the boundaries by the fluctuating flows. The computations indicated that the former was larger in magnitude and tended to increase the $0(G^4a^8)$ mean flow while the latter tended to decrease it.

Solutions can also be found for rigid-free boundaries, where $u = \partial u/\partial z = 0$ at top, $u = w = 0$ at bottom. This reduces to the boundary conditions for the fluctuating flows:

$$\psi = \psi_z = 0 \text{ at } z = -\tfrac{1}{2}, \quad \psi = \psi_{zz} = 0 \text{ at } z = \tfrac{1}{2}. \tag{3.2.16}$$

Thermal boundary condition will be equation (3.1.7) as before. For zero Prandtl number, fluctuations to order 1 and a^2 are found by integrating equations (3.2.2) and (3.2.6)

$$\psi_0 = \frac{G}{4!}\cos(x+Ut)\left[z^4-\frac{1}{2}z^3-\frac{3}{2_2}z^2+\frac{1}{2^3}z+\frac{2}{2^4}\right] \tag{3.2.17}$$

and

$$\psi_1 = -\frac{GU\sin(x+Ut)}{6!}\left[z^6-\frac{3}{2\cdot 2}z^5-\frac{15}{2\cdot 2^2}z^4+\frac{9}{2^3}z^3+\frac{18}{2^4}z^2-\frac{15}{2\cdot 2^5}z - \frac{23}{2\cdot 2^6}\right]. \tag{3.2.18}$$

Boundary conditions for the mean flow are $\psi_z = \psi_{zz} = 0$ at $z = -\frac{1}{2}$ and $\psi_{zz} = 0$ at $z = \frac{1}{2}$. A fourth boundary condition is that vertical velocity is zero, but this is automatically satisfied by a mean flow. The value of $\bar{\psi}_2$ is therefore arbitrary to an additive constant but this is unimportant in determining the mean flow which is a first derivative of $\bar{\psi}_2$. It is

$$\frac{\partial\bar{\psi}_2}{\partial z} = \frac{G^2U}{2\cdot 6!4!}\left[-\frac{1}{5}z^{10}+\frac{1}{2\cdot 2}z^9+\frac{9}{8\cdot 2^2}z^8-\frac{17}{7\cdot 2^3}z^7-\frac{5}{2\cdot 2^4}z^6+\frac{24}{5\cdot 2^5}z^5 + \frac{11}{4\cdot 2^6}z^4-\frac{5}{2^7}z^3-\frac{3}{2\cdot 2^8}z^2+\frac{7}{2\cdot 2^9}z+\frac{95}{56\cdot 2^{10}}\right]. \tag{3.2.19}$$

Surface flow at the top is

$$\bar{u}/U = G^2a^4/5\cdot 8!2^6 = 0.77\times 10^{-7}G^2a^4 \tag{3.2.20}$$

Only even powers of z contribute to the total average flow which is found to be

$$\langle u\rangle/U = 27(G^2a^4/16\cdot 11!) \tag{3.2.21}$$

which agrees with a similar analysis by Hinch (1971).

3.3. Surface Tension Generated Flows

In laboratory experiments with length scales of order 1 centimeter or less and the upper surface of a liquid exposed, there is the possibility of surface tension effects. We seek here the contribution of temperature dependent surface tension by expanding $S = S_0(1-\beta T)$. The upper tangential stress condition becomes, in dimensional form

$$\left(\mu\frac{\partial u}{\partial z} = -S_0\beta\frac{\partial T}{\partial x}\right)_d$$

(see Levich and Krylov, eq. 4 (1969)).
This is transformed to the dimensionless form

$$\left(\frac{\partial^2\psi}{\partial z^2} = -S\frac{\partial T}{\partial x}\right)_n, \quad \text{where} \quad S \equiv \frac{S_0\beta\Delta TL}{\nu\mu}. \tag{3.3.1}$$

The upper normal stress condition remains unchanged to order one. Using zero tangential stress at the bottom boundary, zero vertical velocity above and below and the usual temperature condition (equation (3.1.7)), and ignoring the buoyancy term proportional to G, the zeroth order equations (3.2.1) and (3.2.2) yield,

$$T_0 = \sin(x+Ut), \tag{3.3.2}$$

$$\psi_0 = \frac{-S}{4}\left[z^3+\frac{z^2}{2}-\frac{z}{2^2}-\frac{1}{2^3}\right]\cos(x+Ut) \tag{3.3.3}$$

The order a^2 temperature boundary condition is $T_1 = 0$ at $z = \pm\frac{1}{2}$, and hence it makes no surface traction. Velocity to first order is found using equation (3.2.6). Ignoring the buoyancy term, this yields,

$$\psi_1 = \frac{SU}{4\cdot 20}\left[z^5+\frac{5}{3}\frac{z^4}{2}-\frac{14}{3}\frac{z^3}{2^2}-\frac{6z^2}{2^3}+\frac{11}{3}\frac{z}{2^4}+\frac{13}{3\cdot 2^5}\right]\sin(x+Ut). \tag{3.3.4}$$

Mean flow is

$$\frac{\partial\bar{\psi}_2}{\partial z} = \frac{S^2U}{20\cdot 32}\left[-\frac{1}{4}z^8-\frac{2}{3}\frac{z^7}{2}+\frac{1}{9}\frac{z^6}{2^2}+\frac{26}{15\cdot 2^3}z^5+\frac{7}{6\cdot 2^4}z^4-\frac{10}{9\cdot 2^5}z^3 - \frac{5}{3\cdot 2^6}z^2-\frac{2}{3\cdot 2^7}z-\frac{13}{180\cdot 2^8}\right]. \tag{3.3.5}$$

The top surface flow is

$$\frac{\bar{u}}{U} = \frac{1}{8(5!)^2}S^2a^4 = 0.87\times 10^{-5}S^2a^4. \tag{3.3.6}$$

Even powers contribute to the average flow, which is

$$\frac{\langle u\rangle}{U} = \frac{9S^2a^4}{6!7!} = 0.248\times 10^{-5}S^2a^4. \tag{3.3.7}$$

The numerical coefficients in equations (3.3.6) and (3.3.7) are approximately two orders of magnitude larger than those for buoyancy driven mean flows equations (3.2.20) and (3.2.21). This arises due to the six-times larger coefficient in front of the zeroth order circulation (equation (3.3.3)), and the nine-times larger coefficient in front of the first-order circulation (equation (3.3.4)), plus the fact that each of those equations is one power lower in z than the buoyancy driven flows. One therefore is led to the conclusion that surface tension forces of comparable size to buoyancy forces are many times more effective in generating mean flows.

4. Comparison of experiment with theory and discussions

Before comparing experiment and theory a typical signal was Fourier analyzed, the one chosen being a compromise between the extremely jagged signal shown in figure 3 (which was for the deep run number 48), and the smoothest signals obtained in the experiments (which were obtained for the most rapid flame speeds). The final signal selected was run #26, and it was found that the first seven harmonics had amplitudes 0.791, 0.317, 0.193, 0.069, 0.053, 0.00306, and 0.0030 times as large as the total temperature difference. A correction factor to the theoretical equations was determined by using the formula

$$F_c = \sum_{n=1}^{7} A_n^2 n^4$$

where A_n is the nth amplitude. It totalled 8.2, most contributions coming from the first five harmonics. The formula can be deduced by inspection of the theory in part 3. Although F_c is expected to be a function of heater speed and depth of the mercury, this number appeared to be typical because visual inspection revealed only small differences in qualitative shape of the various thermal signals.

In comparing the results with theory, values of the physical properties of mercury, with the exception of the surface tension temperature coefficient, were taken from the Handbook of Chemistry and Physics (1961). Kinematic viscosity was taken as $\nu = 0.00116\ \text{cm}^2/\text{second}$, thermal diffusivity was taken to be $\kappa = 0.043\ \text{cm}^2/\text{second}$, Prandtl number was 0.027, and the coefficient of expansion was taken as $\alpha = 0.000181°\text{C}^{-1}$. It was difficult to determine a value of surface tension coefficient for the mercury–water interface, as direct data was not available. Furthermore, the presence of oxides and impurities would surely alter the exact value. It is well-known that ordinary tap water can be expected to have a surface tension almost 50% below the value of pure water. A safer procedure was to calculate two extreme values—a high and a low from data on surface tension coefficients of mercury in contact with a

variety of materials. To this end, data from the International Critical Tables (1926) was used. The value 0.26 dyne-cm/°C for Hg–Benzine at 20°C was the largest value found for any mercury interface; while 0.09 dyne-cm/°C for Hg–Octane at 40° was the smallest value found in the temperature range between 20° and 40°C. Since these values bracket the temperature coefficients for Hg–vacuum, Hg–Hg vapor, Hg–air, and H_2O–air, it is reasonable to expect the true experimental value to be within these limits.

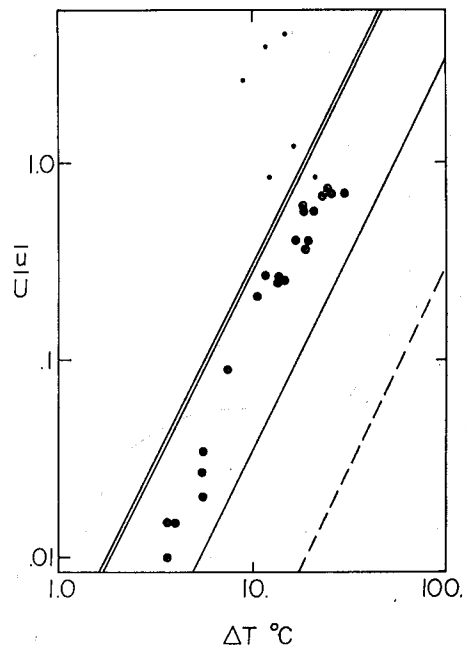

FIGURE 6 Summary of experimental measurements of mean flow compared with flame speed, as a function of ΔT. The data in large dots are for a depth of 0.35 cm, the data in small dots are for deeper depths. The dashed line is for rigid-free buoyancy driven convection $\bar{u}/U = 3.05 \times 10^{-5} \Delta T^2$. The solid line is for the minimum surface tension prediction $\bar{u}/U = 3.46 \times 10^{-4} \Delta T^2$ while the double solid line is for the maximum surface tension prediction $\bar{u}/U = 29.0 \times 10^{-4} \Delta T^2$.

The experimental data are plotted in figure 6. Using the physical values for mercury mentioned previously, a depth of 0.35 cm, and the correction factor F_c, equation 3.2.20 for buoyancy-driven flow is found to be $3.05 \times 10^{-5} \Delta T^2$ and is shown as a dashed line, while equation 3.3.6 for surface tension driven flow is $29.0 \times 10^{-4} \Delta T^2$ for the maximum surface tension coefficient, shown as a double line, and $3.46 \times 10^{-4} \Delta T^2$ for the minimum surface tension coefficient, shown as a single line.

Qualitatively, the 0.35 cm-deep data shows that $\bar{u}$ is proportional to $U\Delta T^2$ for almost a decade span in temperature, and more than a decade span in heater speed. This conforms to the slow-speed buoyancy-driven predictions of Davey and was a motivation for the expansion procedure in Part 3. Quantitatively, we note that the 0.35 cm-deep data greatly exceed the buoyancy-driven predictions, but are bracketed by the surface tension predictions. Since it is likely that additional corrections will decrease the predictions, the data indicate that surface tension generates the observed flows in mercury.

For rapid heater speeds with buoyancy-driven flows, the speed would be proportional to the parameter group $U^{-4}\Delta T^2$, as predicted in the high speed limit of Davey, and in the strong streaming predictions of Hinch and Schubert at very large Reynolds number. A similar behavior could be expected for surface tension driven flows; however, it was not possible to attain this limit because temperature amplitudes were negligibly small at such speeds.

Another interesting possibility was pointed out by Malkus—that a constant heat flux boundary condition could lead to a mean flow at vanishing heater speeds as a finite amplitude instability. Indeed, these mercury experiments with heat from intense radiative bulbs have a very close approximation to a constant heat flux boundary condition. Unfortunately, no mean flow was ever observed when the heater was stopped, even if the mercury was initially moving very rapidly. However, the spin-down time of artificially started mean flows was observed to increase so that possibly the critical parameters necessary to start a self-reinforcing mean flow were not exceeded by the experiment. In addition, possibly the wavelength of the mercury was not small enough, or possibly the surface tension driven motions convect heat laterally more effectively than the mean flow advection.

Data for the deeper mercury depths lie higher than the shallow ones, but appear to be smaller than surface tension theory predicts. Experimental measurements of the spin-down of mercury in the channel showed that for depths above 0.35 cm the spin-down time was proportional to $(L^2/\bar{U})^{\frac{1}{2}}$. This behavior is characteristic of flows along a curved channel where, for sufficiently rapid flows, there is a secondary circulation in a radial direction due to centrifugal forces. Because of the engineering importance of such flows, extensive measurements have been made of the "friction factor" generated by the radial motions. The experimental times mentioned above which were proportional to $(L^2/\bar{U})^{\frac{1}{2}}$ agreed well with the tables in Rosenhow and Choi (1961), p. 60. It was consequently felt that the data for deeper mercury depths, although showing the interesting rapid flows, would not easily be reconciled with theory.

The data indicates that surface tension generates the observed flows in mercury. Mean flows have also been observed by Fultz and Stern, and there

are some unpublished observations by Hinch of water heated internally, which exhibited rapid flows. The theory done here, which may not apply to the above cases due to the relatively large Prandtl number of water, indicates that surface tension is the dominant stress generating mechanism if $S/G > 0.1$, i.e., if $S_0\beta/g\rho_0\alpha L^2 > 0.1$, which is certainly not true in the experiments of Fultz or Hinch, but was marginally satisfied in Stern's experiments.

Two experiments have been done to independently test the idea of a surface tension driven circulation. In the first, an intense lamp was placed over a channel filled with water. Presumably, a considerable amount of infrared energy would be absorbed near the very top of the water, and a lateral temperature gradient should exist on the top surface, hence a surface tension gradient could be expected. Unfortunately, due to the high specific gravity of mercury, the value of S for water at the same ΔT is about 0.1 that of mercury. However, experiments on such an apparatus yielded values of $\bar{u}/U$ up to 0.05, and the magnitudes are compatible with the surface tension theory. In a second experiment most of the mercury top surface was covered by a solid sheet of aluminum, and the heater was run at a speed and amplitude which had previously generated a considerable mean flow. Measurements with the balanced vertical metal rod placed through a hole in the sheet indicated only a very small mean flow, if any.

The theoretical development shows that the coefficients in front of the various terms are small, and this is the reason the expansion must be justified *a posteriori*. We note that for the shallow depth of 0.35 cm the maximum value of Ga^2 was approximately 200, maximum Ua^2 was 8.5, and maximum Sa^2 was 1830. The first-order buoyancy-driven surface flow for the rigid-free case (equation (3.2.8)) was approximately 0.43 times as large as the zeroth order flow (equation (3.2.4)), while the first-order surface-tension-driven flow equation (3.3.4)) was approximately 0.86 as large as the zeroth order flow (equation (3.3.3)). Since other datum points lay below this extreme, most can be considered to be safely inside the region of validity of the "slow flow" assumption, and hence can be considered small. Finally, we note that the final solution for the rigid–rigid mean flow to eighth order in "a" is given in equation (3.2.10) whose second and third terms are 2.0×10^{-2} and approximately 10^{-4} as large as the first term, respectively. In view of the fact that the $0(G^4a^8)$ correction in equation (3.2.21) had a coefficient approximately as large as the coefficient in front of the equation, one can expect a similar result in the surface tension solution, and can conclude that the theory will begin to become invalid as mean flow approaches one. The only benefit to be gained by pursuing such a scheme to higher orders is to see the trend of the new processes emerging. Strictly speaking, when the higher orders are valid, each successive order can be expected to be even larger. However, other

theoretical techniques exist which can correctly analyze the rapid flow regimes. These have been used by Hinch and Schubert (1971).

In closing, it must be noted that it has not been possible to link the most rapid mean flows observed with theory, and unhappily all flows which have been predicted by theory have been slower than the heater speed. Therefore, it is not possible to deduce the actual mechanisms acting in the cases where mean flows are more rapid than the heater speed. However, we note that although the experimental flow is generated from a surface tension traction at the top surface, the Reynolds stress generated by the phase lag of the moving vorticity field is identical to that in the buoyancy driven flows. It therefore can be a useful guide to understanding many of the interesting Reynolds stress-generating flows in nature.

Acknowledgments

I am greatly indebted to the late Paul Cox for precise construction of the experimental apparatus. Thanks are also due to Gerald Schubert and Richard Young for informative discussions. Support was provided by the National Science Foundation, Atmospheric Science section under Grant No. GA-19605.

References

Davey, A., "The motion of a fluid due to a moving source of heat at the boundary," *J. Fluid Mech.*, **29,** 137–150 (1967).

Fultz, D., "Studies in experimental hydrodynamics (I)." Final Report, Hydrodynamics Lab., Univ. of Chicago, B37–B40 (1956), in *Meteor Monographs*, **4,** 36 (1959).

Handbook of Chemistry and Physics, 43rd ed. The Chemical Rubber Publishing Company, Cleveland, Ohio (1961).

Hinch, J. and Schubert, G., "Strong streaming induced by a moving thermal wave," *J. Fluid Mech.*, **47,** 291–304 (1971).

Hinch, J., "The moving flame: a dynamical model for Venus's four-day circulation." Essay, recipient of a Smith and Rayleigh Prize (1971).

International Critical Tables, Vol. **4,** 432–450, McGraw-Hill, New York (1926).

Levich, V. G. and Krylov, V. S., "Surface tension driven phenomena," *Annual Review of Fluid Mechanics*, **1,** 292–316 (1969).

Malkus, W. V. R., "Hadley-Halley circulation on Venus," *J. Atmos. Sci.*, **27,** 529–535 (1970).

Rosenhow, W. M. and Choi H. Y., *Heat, Mass and Momentum Transfer*, Prentice Hall, Englewood Cliffs, New Jersey (1961).

Schubert, G. and Whitehead, J. A., "The moving flame experiment with liquid mercury: possible implications for the Venus atmosphere," *Science*, **163,** 71–72 (1969).

Schubert, G., "High velocities induced in a fluid by a traveling thermal source," *J. Atmos., Science*, **26,** 767–770 (1969).

Starr, V. P., *Physics of Negative Viscosity Phenomena*, McGraw-Hill, New York (1968).

Stern, M. E., "The moving flame experiment," *Tellus*, **11,** 175–179 (1959).

Thompson, R., "Venus' general circulation is a merry-go-round", *J. Atmos. Sci.*, **27,** 1107–1116 (1970).

Geophysical Fluid Dynamics, 1972, Vol. 3, pp. 181–209
© 1972 Gordon and Breach Science Publishers Ltd.
Printed in Great Britain

A Laboratory Study of Baroclinic Instability

J. E. HART

Department of Astro-Geophysics
University of Colorado
Boulder, Colorado, U.S.A.

(*Received August 2, 1971*)

Experimental and theoretical results are presented for a simple system which exhibits baroclinic instability. We consider the motion of two immiscible fluids with densities ρ_1 and ρ_2 contained in a cylinder rotating with angular frequency Ω. The motion is driven by a contact lid rotating with frequency $\Omega+\omega$. In this paper Ω, ω, $2(\rho_2-\rho_1)/(\rho_2+\rho_1)$, and the geometry are such that the interface does not intersect the "ground" (e.g. an almost horizontal boundary). The motions are described by two-layer quasi-geostrophic equations which are identical, except perhaps for the presence of interfacial friction and tension, with those used in meteorology and oceanography. For small enough internal Froude number $F = 4\Omega^2L^2/(g(\Delta\rho/\rho)H)$ or small enough Rossby number $\varepsilon = \omega/2\Omega$ the flow is steady and axisymmetric, the velocity field in each layer being determined primarily by frictional effects in top, bottom, and interfacial Ekman layers. For certain (F, ε) the flow becomes non-axisymmetric. The transition points for the case where the basic potential vorticity gradient is due to interface slope alone have been carefully measured and are in very good agreement with a linear instability theory which neglects sidewall effects. Some preliminary observations of supercritical motion, which include repeatable amplitude and wavenumber vacillation, are reported.

1. Introduction

For many years it has been recognized that the transformation of available potential energy into kinetic energy by eddy motions plays a major part in the dynamics of the atmosphere and the ocean. A great deal of effort has been expended on all fronts, observational, theoretical, computational, and experimental, to obtain an understanding of this process, and of the details of the motions involved. Much of the by now vast body of literature on this subject has been recently reviewed in the monograph by Lorenz (1967). The analyses of Charney (1947) and Eady (1949) indicated that typical large scale stratified shear flows in the earth's atmosphere would be unstable to a class of disturbances called baroclinic waves, which are characterized by a conversion